REPORT DOCUMENTATION PAGE

Form Approved
OMB No. 0704-0188

1. REPORT DATE *(DD-MM-YYYY)*	2. REPORT TYPE	3. DATES COVERED *(From - To)*
3/27/2017	Final	5/14/2014-12/31/2016

4. TITLE AND SUBTITLE

Simultaneous Strain and Temperature Measurement Using a Single Fiber Bragg Grating Coated with a Thermochromic Material

5a. CONTRACT NUMBER

5b. GRANT NUMBER
N00014-14-1-0636

5c. PROGRAM ELEMENT NUMBER

6. AUTHOR(S)

Haiying Huang

5d. PROJECT NUMBER

5e. TASK NUMBER

5f. WORK UNIT NUMBER

7. PERFORMING ORGANIZATION NAME(S) AND ADDRESS(ES)

University of Texas Arlington
500 W. First Streert, WH211
Arlington, TX 76019

8. PERFORMING ORGANIZATION REPORT NUMBER

9. SPONSORING/MONITORING AGENCY NAME(S) AND ADDRESS(ES)

Dr. Ignacio Perez
Program Officer for PMC and NDE, Office of Naval Research
Code 332, rm 649, Arlington VA, 22203

10. SPONSOR/MONITOR'S ACRONYM(S)

11. SPONSOR/MONITOR'S REPORT NUMBER(S)

12. DISTRIBUTION/AVAILABILITY STATEMENT

DISTRIBUTION STATEMENT A: Approved for public release. Distribution is unlimited

13. SUPPLEMENTARY NOTES

14. ABSTRACT

The objective is to demonstrate simultaneous strain and temperature measurement using a single Fiber Bragg Grating (FBG). We developed two techniques to achieve this objective based on the principle of spectral bandwidth modulation. This project supported two graduate students and resulted in one journal paper published, one journal manuscript submitted, two conference presentations, and one master's thesis.

15. SUBJECT TERMS

16. SECURITY CLASSIFICATION OF:			17. LIMITATION OF ABSTRACT	18. NUMBER OF PAGES	19a. NAME OF RESPONSIBLE PERSON
a. REPORT	b. ABSTRACT	c. THIS PAGE			Haiying Huang
U	U	U	SAR	12	19b. TELEPHONE NUMBER *(Include area code)* 817-272-0563

Report Information

Name: Haiying Huang
Organization: University of Texas Arlington
Email: huang@uta.edu

Contract Information
Contract Number: N00014-14-1-0636
Contract Title: : Simultaneous Strain and Temperature Measurement Using a Single Fiber Bragg Grating with a Thermochromic Coating
Program Officer: Dr. Ignacio Perez
CO-PI Information: Yi Hong, Dept. of Bio-Engineering, University of Texas Arlington

Abstract: the objective of this project is to demonstrate simultaneous strain and temperature measurement using a single Fiber Bragg Grating (FBG). We discovered that the spectral bandwidth of a conventional FBG sensor can be modulated by coating the FBG sensor with a thermochromic material or embedding the FBG sensor in a composite laminate. Since the bandwidth modulation of the FBG sensor is temperature and strain dependent, we introduced the FBG spectral bandwidth as an additional sensor parameter that can be combined with the Bragg wavelength for simultaneous strain and temperature measurements. Thermal-mechanical tests were conducted to validate this principle and a data analysis algorithm was developed to extract the temperature and strain values simultaneously from the spectral parameters of the FBG sensor. For an FBG sensor coated with thermochromic material, the measurement errors for the axial load and the temperature were found to be +/- 4 gm and +/-4^{o}C, respectively. For an FBG sensor embedded in a composite laminate, the measurement errors, within one standard deviation, for the strain and temperature measurements were found to be +/- 62 με and +/- 1.94^{o}C, respectively. This project supported two graduate students and resulted in one journal paper published, one journal manuscript submitted, two conference presentations, and one master's thesis.

Technical Section

1. ***Simultaneous load and temperature measurement using Lophine – coated Fiber Bragg Gratings***

The coating of a photosensitive step index single mode fiber (Corning, NA = 0.28) was stripped for a length of 30 mm and a 6.35 mm long straight Fiber Bragg grating (FBG) was inscribed using a 193 nm excimer laser (Bragg Star Industrial-LN 1000 FT) and a phase mask (1071.5 nm). The grating was written at a uniform scanning speed of 0.37 mm/s while the laser power was controlled at 5 *mJ* with a repetition of 800 Hz. We selected 2,4,5-triphenylimidazole (Lophine) as the transducing element, because it is anisotropic, nontoxic, hydrophobic. Having a low melting point of 275–277 °C, it enables us to coat, un-coat and re-coat the FBGs so that the repeatability of the sensor response can be evaluated. In addition, it is very easy to machine the sample and control the height of the coating. In order to coat the FBG sensors with molten Lophine and to control the coating thickness, a mold was designed. As shown in figure 1.1(a), the mold consists of a base plate and two vertical plates. The distance between the two vertical plates was controlled by inserting spacers with the desired thickness. Once the mold was adjusted properly, an optical fiber was placed at equal distances from the vertical plates with the help of a microscope and taped in position using high temperature tapes. To melt the Lophine, a beaker was heated up to 475°C using a hot plate and Lophine powder was added slowly to the heated beaker (see figure 1.1(b)). Once sufficient molten Lophine was obtained, the molten Lophine was poured carefully into the space between the two vertical plates of the mold. As it cools down, the molten Lophine formed a recrystallized Lophine block with the FBG encapsulated inside, as shown in figure 1.1(c). The Lophine block removed from the mold is shown in Figure 1.1(d), which has rough edges and the optical fiber is not centered. To smoothen the edge and produce a Lophine block with the optical fiber in the center, the edges of the block were brought in contact with a heated metal plate to remove any excessive Lophine (see figure 1.1(e)). As shown in figure 1.1(f), the FBG sensor is located at the center of a Lophine block with a uniform thickness of 1.5 mm, a height of 3.46 mm, and a length of 46 mm.

The reflectance spectra of the FBG before and after coating were measured using an optical spectrum analyzer (OSA) with a resolution of 0.2 nm. As shown in figure 1.2, the output of the OSA light source, i.e. an edge-emitting LED (EELED), was routed to the FBG sensor through a 50:50 single mode optical fiber coupler so that

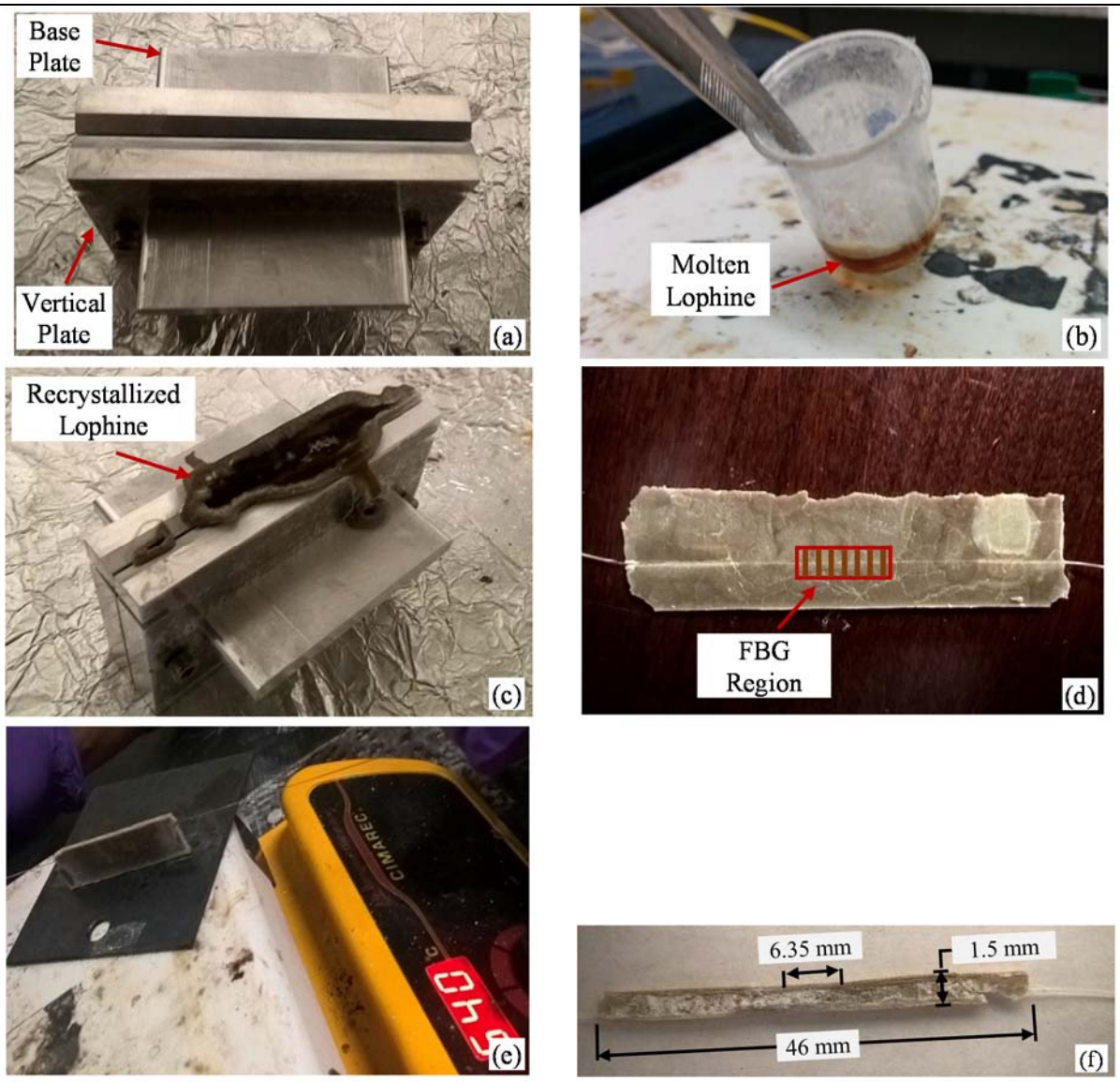

Figure 1.1. Coating Fiber Bragg Grating with recrystallized Lophine: (a) mold for thickness control; (b) melt Lophine in a beaker using a hot plate; (c) recrystallize Lophine in the mold; (d) recrystallized Lophine block with FBG encapsulated inside; (e) reduce the height of the recrystallized Lophine block using a heated plate; (f) final Lophine – coated FBG sample.

a portion of the light reflected by the FBG sensor can be routed to the input of the OSA. An Excel Visual Basic (VB) Program was developed to record the reflected spectrum from the OSA. The FBG spectra reflected by a Lophine coated FBG is compared with that of a bare FBG in figure 1.3. The bare FBG produced a typical reflectance spectrum with a sharp peak while the coated FBG produced a reflectance spectrum with a much broader peak. In addition, the spectrum produced by the Lophine-coated FBG also shifted to a shorter wavelength. In order to quantify these observed changes, a MATLAB program was developed to extract two spectral parameters, i.e. the central Bragg wavelength and bandwidth, from the measured reflectance spectra. Two wavelengths, i.e. the low cut-off and high cut-off wavelengths, were determined as the wavelengths at which the intensity of the spectrum is 8 dB below the peak intensity. The central Bragg wavelength is then calculated as the average of these two wavelengths while the bandwidth is calculated as the difference between these wavelengths. For the bare FBG sensor, the central Bragg wavelength was found to be 1550.255 nm and the bandwidth is 0.447 nm. In contrast, the Lophine-coated FBG has a central wavelength of 1549.567 nm and a bandwidth of 1.561 nm. The

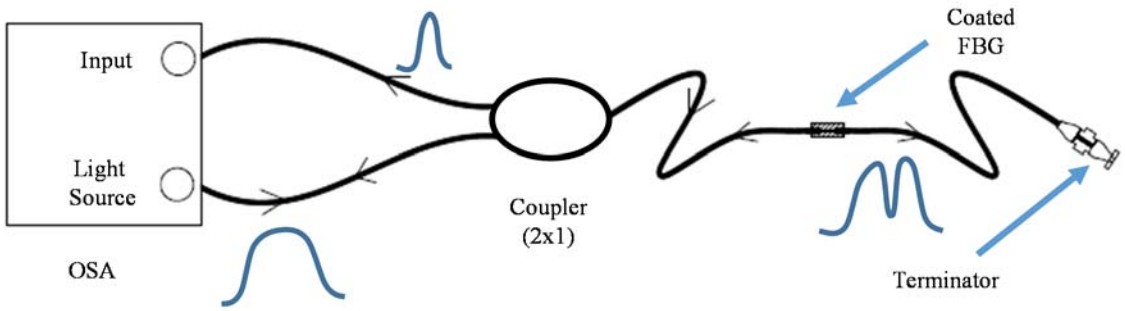

Figure 1.2. Experimental setup for measuring the reflectance spectrum of FBG sensor.

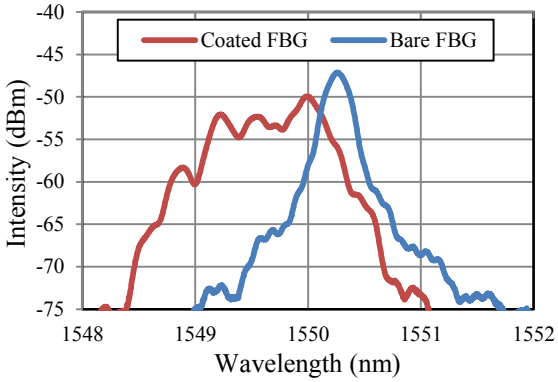

Figure 1.3. Reflectance spectra of the FBG before and after Lophine coating.

shift of the central wavelength toward a shorter wavelength indicated that the coating compresses the FBG. The broadening of the reflectance spectrum is likely due to the non-uniformity of the compressive residual stress introduced by the Lophine coating.

The Lophine-coated FBG sensor were tested under simultaneous thermal and mechanical loadings inside a temperature-controllable incubator, as shown in figure 1.4. The optical fiber was hung vertically by gluing its top portion on a flat fixture. The lower portion of the optical fiber was reinforced with another flat plate so small weights can be hung. The weight was increased from 0 to 80 gm in an increment of 20 gm. Therefore, the axial load experienced by the FBG sensor is the hanging weight plus the weight of the lower flat plate, which is 15.6 gm. Under each weight, the temperature of the incubator was heated from 30 to 60°C in an increment of 5°C. The reflectance spectrum of the FBG sensor was acquired and stored for each weight and temperature combination.

The responses of the FBG spectra to the temperature changes, under two different weights, is shown in figure 1.5. For both cases, the reflectance spectrum shifted to the right while the peak narrowed as temperature increased. The central Bragg wavelengths and the bandwidths extracted from the reflectance spectra under constant

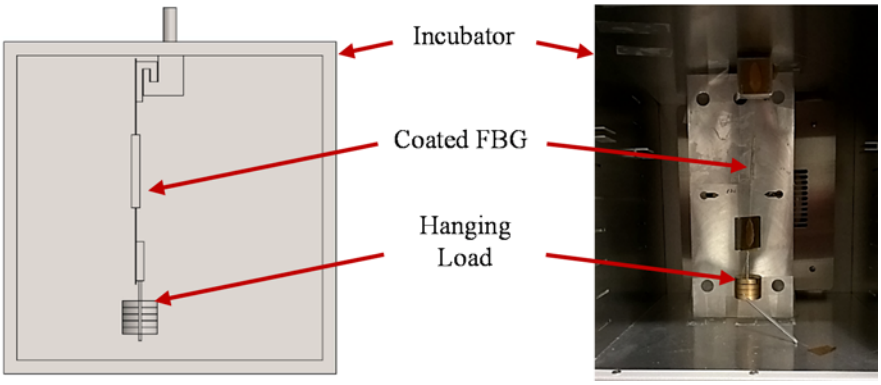

Figure 1.4. Experimental set-up for thermal-mechanical testing of Lophine-coated FBG sensor.

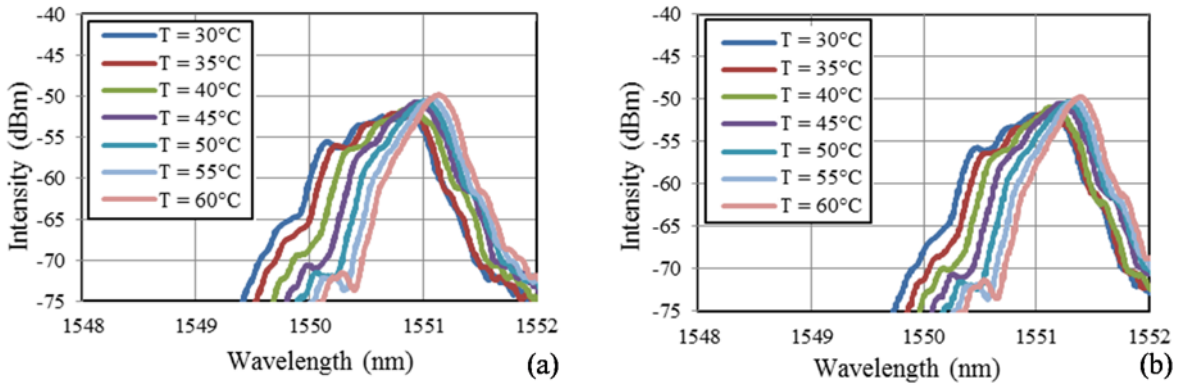

Figure 1.5. Change of FBG spectrum with temperature under two different loads; (a) 20 gm and (b) 40 gm.

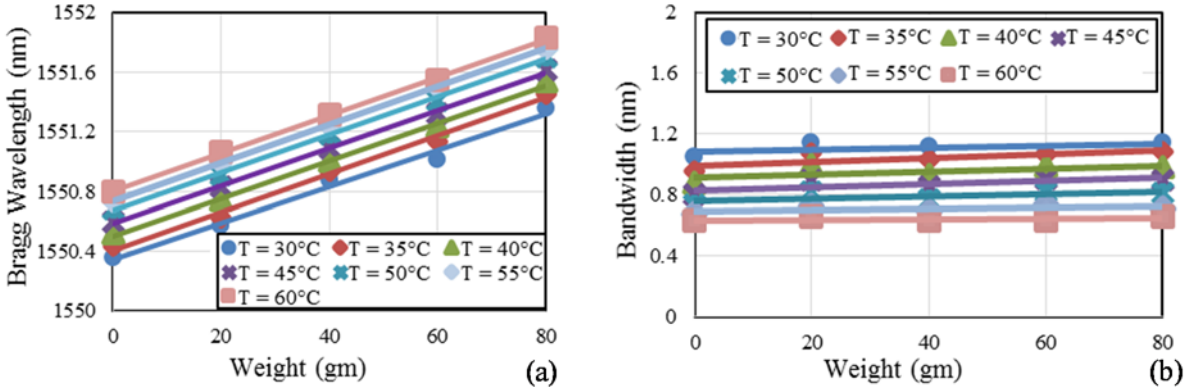

Figure 1.6. The shift in (a) central Bragg wavelength and (b) bandwidth with the applied weight under different temperatures.

temperatures are plotted versus the axial load in figure 1.6. Both the central wavelength and the bandwidth appear to be linearly proportional to the temperature as well as the axial load. Therefore, they can be curve fitted using linear functions, i.e.

$$BW(T,W) = -0.01591\,T + 0.00073\,W + 1.559\,, \tag{1.1}$$

$$\lambda_B(T,W) = 0.01619\,T + 0.01263\,W + 1550\,, \tag{1.2}$$

where T is the temperature, W is the axial load, BW is the measured bandwidth, and λ_B is the measured Bragg wavelength. The coefficients of linear equations were found using a curve fitting tool available in MATLAB. Once equations (1.1) and (1.2) are established, the axial load and temperature corresponding to each FBG spectrum can then be inversely determined from the measured FBG bandwidth and Bragg wavelength as

$$\begin{bmatrix} T \\ W \end{bmatrix} = \begin{bmatrix} -0.01591 & 0.00073 \\ 0.01619 & 0.01263 \end{bmatrix}^{-1} \left(\begin{bmatrix} BW \\ \lambda_B \end{bmatrix} - \begin{bmatrix} 1.559 \\ 1550 \end{bmatrix} \right) \begin{pmatrix} ^\circ C \\ gm \end{pmatrix}. \tag{1.3}$$

The differences between the axial load and temperature determined using equation (1.3) and their actual values are presented in figure 1.7. For temperature, the measurement errors are larger at lower temperatures, which are within $\pm 4^\circ$C, but the errors reduced to around $\pm 2^\circ$C for higher temperatures. On the other hand, the measurement errors for the axial load appear to be independent of the applied load. Except one outlier that produced an error of -9.7 gm, the measurement errors of the axial load are within ± 4 gm. Assume the strain sensitivity of a standard FBG is 1.2 pm/με [12] and the measured load sensitivity of 13.4 pm/gm from our experiment, we estimated that 1 gm of axial load is equivalent to 11.2 με. Therefore, the corresponding strain errors are within $\pm$ 44.8 με.

The thermal and mechanical responses of the bare FBG was tested before the coating process and after the Lophine coating was removed. We found that the FBG responses were repeatable after multiple coating and uncoating processes, which indicated that the molten Lophine does not cause any irreversible effect on the FBG.

2. ***Simultaneous strain and temperature measurement using a single fiber Bragg grating embedded in a composite laminate***

An FBG is a periodic modulation of RI inscribed in the core of a single mode fiber (SMF). When a guided light encounters an FBG in its path, a narrow band of the light is reflected back, as shown in figure 2.1(a). For a traditional SMF with a symmetric fiber core, light along different polarization directions experiences the same Bragg conditions. Therefore, the reflectance spectrum of the FBG carries a single resonance peak that is centered at the Bragg wavelength, as shown in figure 2.1 (b). For an FBG with birefringence, however, the RI of the fiber core is no longer symmetric. As a result, light with different polarization directions encounter different Bragg conditions, i.e.

$$\lambda_{B,x} = 2\, n_{eff,x}\, \Lambda \quad \text{and} \quad \lambda_{B,y} = 2\, n_{eff,y}\, \Lambda, \tag{2.1}$$

in which λ_B is the Bragg wavelength, n_{eff} is the effective RI of the fiber core, and Λ is the grating period. The subscripts x and y represent two perpendicular polarization directions. As a result, the reflectance spectra of such FBG sensors carry polarization–dependent split resonance peaks, as shown in figure 2.1(c). Birefringence, i.e. the difference in the RI of the optical fiber along two perpendicular polarization directions, can be introduced by subjecting the FBG to unsymmetrical mechanical stresses, such as embedding the FBG in composite laminates. The resulting RI of the fiber core can be expressed as

$$n_x = n_{x0} + C\sigma_x \quad \text{and} \quad n_y = n_{y0} + C\sigma_y, \tag{2.2}$$

in which $n_{xo} = n_{yo}$ are stress-free RI of the fiber core, C is the stress-optic coefficient, and σ_x and σ_y represent the principal stresses applied perpendicular to the fiber longitudinal direction. If the difference between σ_x and σ_y is small, the two resonance peaks are closely packed, appearing as a single resonance peak with a broadened bandwidth. For composite materials, the strain applied along the longitudinal direction of the optical fiber and temperature may change the difference between σ_x and σ_y, causing the bandwidth of the resonance peak to change. Since the Bragg wavelength of the reflected FBG spectrum is also sensitive to the longitudinal strain and temperature, combining the spectral bandwidth and the Bragg wavelength enables measuring two physical quantities, e.g. the strain and temperature, simultaneously.

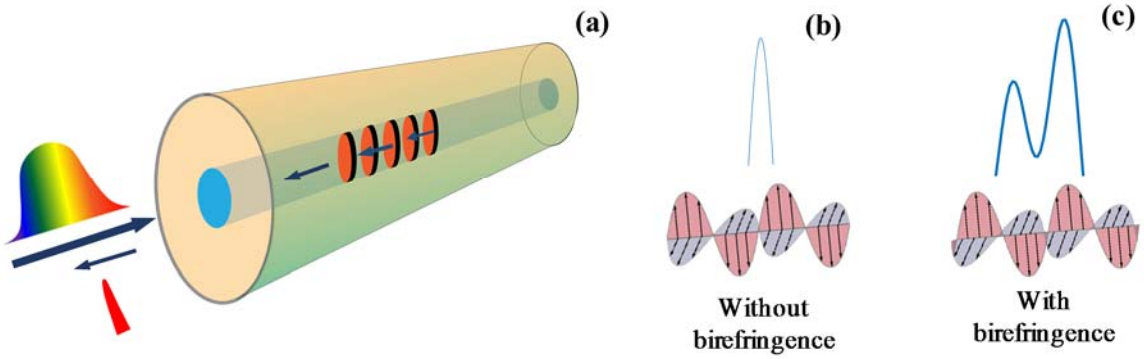

Figure 2.7. Propagation of light in an SMF with an inscribed FBG; (a) schematic of an FBG sensor; (b) reflected spectrum of an FBG without birefringence); (c) reflected spectrum of an FBG with birefringence.

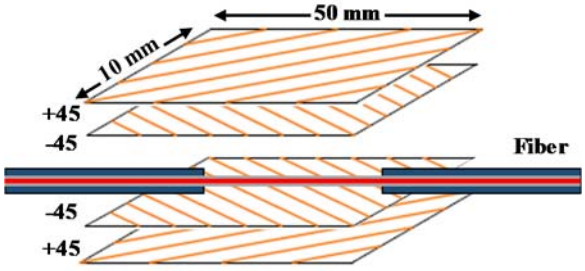

Figure 8.2. Sensor design with an FBG embedded in composite plies.

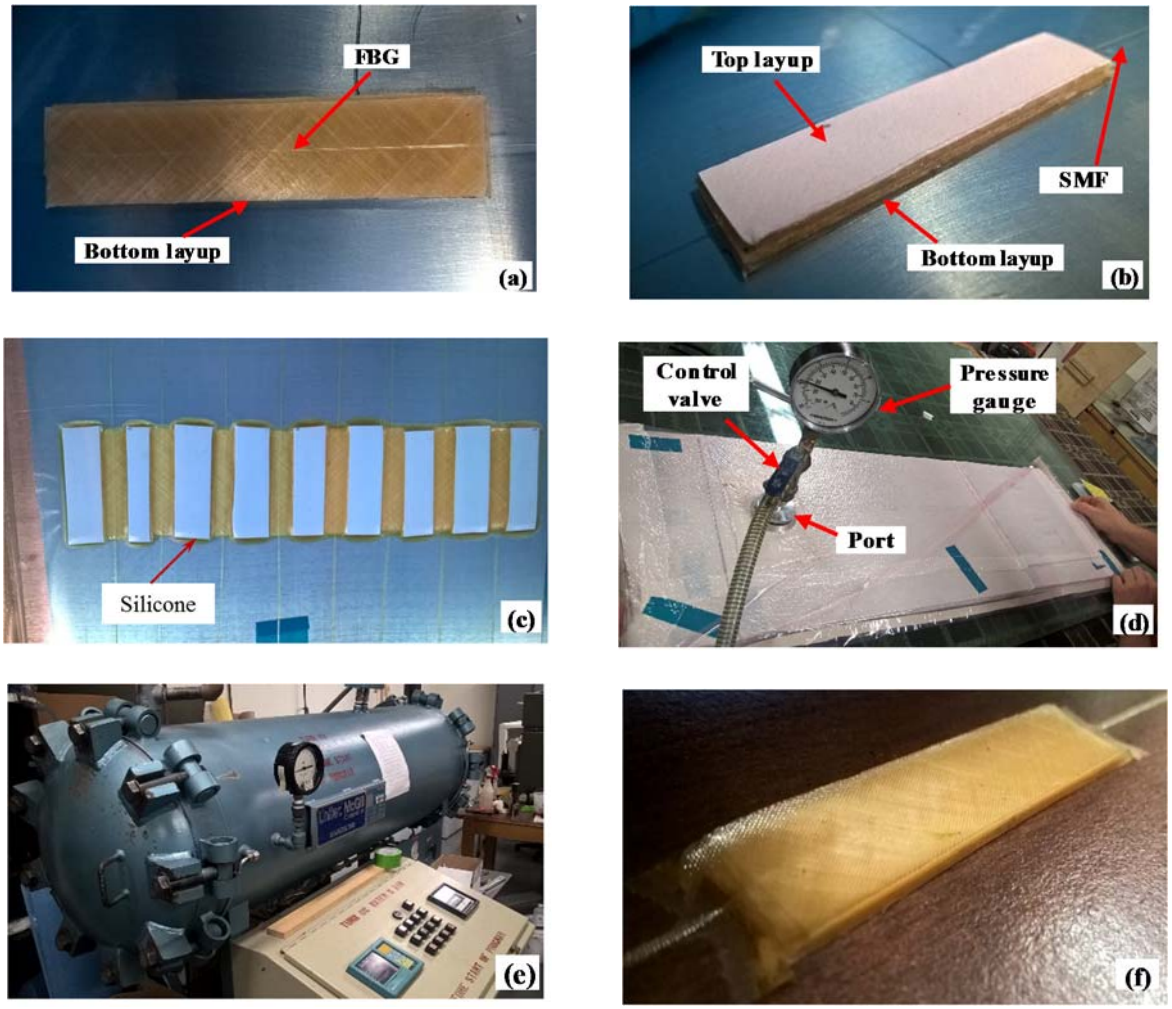

Figure 9. Fabrication process for embedding an FBG sensor in a composite laminate: (a) preparation of bottom layup; (b) sandwiching FBG between top and bottom layup; (c) surrounding layups with silicone at both sides; (d) vacuum bagging sensor package; (e) curing in autoclave; (f) fabricated FBG-composite sensor.

The sensor design is shown in figure 2.2. A conventional FBG sensor is embedded in the center of four unidirectional laminate plies with fibers oriented at an angle of ±45°. Equal numbers of positive and negative plies were used for a balanced configuration. The fabrication process to embed the FBG sensor in the composite laminates (HexPly 8552-2GL) is shown in figure 2.3. The composite laminates were cut to be 50 mm long and 10 mm wide. The layup was prepared by stacking the [±45]s plies with the FBG embedded in the center (see figures 2.3(a) and 2.3(b)). Silicone blocks were placed at both sides of the layup, as shown in figure 2.3(c), to prevent lateral dislocation of the plies, and to avoid stress concentrations during vacuum bagging of the layup. As shown in figure 2.3(d), the layup was inserted into a vacuum bag so that a negative pressure can be applied through the port and control valve using a vacuum pump. Once a constant pressure of -80 kPa was established, the sealed vacuum bag was put inside the autoclave shown in figure 2.3(e). The vacuum-valve of autoclave was then connected to the port of the vacuum bag in order to maintain the constant negative pressure during the cure cycle. The autoclave was programmed to follow the temperature and pressure cycles to ensure the full curing of composite laminate. The sensor, thus developed, was found to be 0.8 mm thick and is shown in figure 2.3(f).

The presence of birefringence after embedding the FBG in the composite laminate was validated using the experimental setup shown in figure 2.4. An unpolarized light, generated using an edge-emitting light-emitting-diode (EELED), was linearly polarized with the help of a polarizer filter (PF). The orientation of the polarized light can then be adjusted using a polarizer controller (PC). The polarized light was routed to the FBG sensor

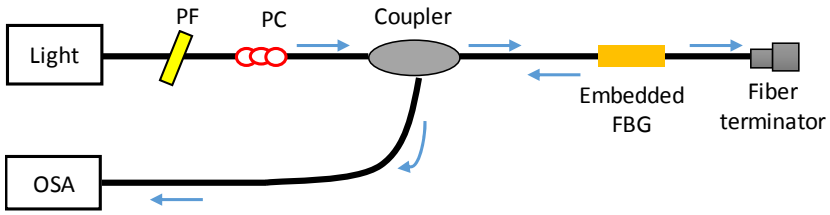

Figure 2.4. Experimental setup for measuring the reflectance spectrum of FBG-composite sensor.

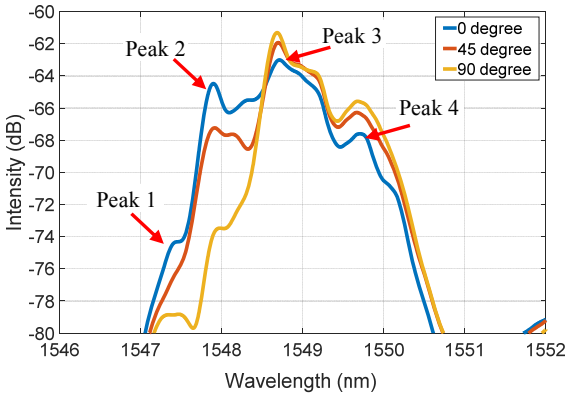

Figure 2.5. Verification of stress induced birefringence by measuring spectral response at different orientations of plain polarized light.

through a 50:50 optical coupler, which also routes the light reflected by the FBG sensor to an optical spectrum analyzer (OSA). The OSA was programmed to have a wavelength resolution of 0.2 nm and the acquired spectrum was saved to a computer with the help of a Visual Basic (VBA) Program developed in Microsoft Excel. The reflectance spectra of the FBG sensor with different polarization directions are shown in figure 2.5. Unlike conventional FBG sensors, whose reflectance spectrum is typically polarization independent, the spectrum of the FBG sensor embedded in the composite contained split peaks that are sensitive to the polarization direction of the interrogation light. As the polarization direction was changed from 0 to 90 degree, the peak at lower wavelengths (peak 1 and peak 2) gradually disappeared while the peaks at higher wavelengths (peak 3 and peak 4) become more dominant. These results verify that the birefringence was introduced to the FBG by embedding it in the composite laminate.

To evaluate the responses of the embedded FBG sensor to thermal and mechanical loadings, the FBG-composite sensor package was bonded on an aluminum dog-bone sample, as shown in figure 2.6(a). The dog-bone sample was designed in compliance with the ASTM standard B557 –15 and has a thickness of 3 mm. A Hysol E-Z Pack epoxy was used as the bonding agent and the bonding was cured at 80°C for 6 hours. The instrumented sample was then annealed and exposed to a tension-relaxation cycle before the actual test was performed. The experimental setup for the thermo-mechanical testing is shown in figure 2.6(b). It consists of a thermostatic chamber integrated with a mechanical tester; both from Shimadzu. Inside the thermostatic chamber, the dog-bone sample was clamped between the jaws of the mechanical tester and an extensometer from Epsilon was installed on top of the sensor patch (see figure 2.7(c)). The temperature of the thermostatic chamber was increased from 35°C to 55°C in an increment of 5°C. At each temperature, the tensile load was varied from 0 N to 3000 N in an

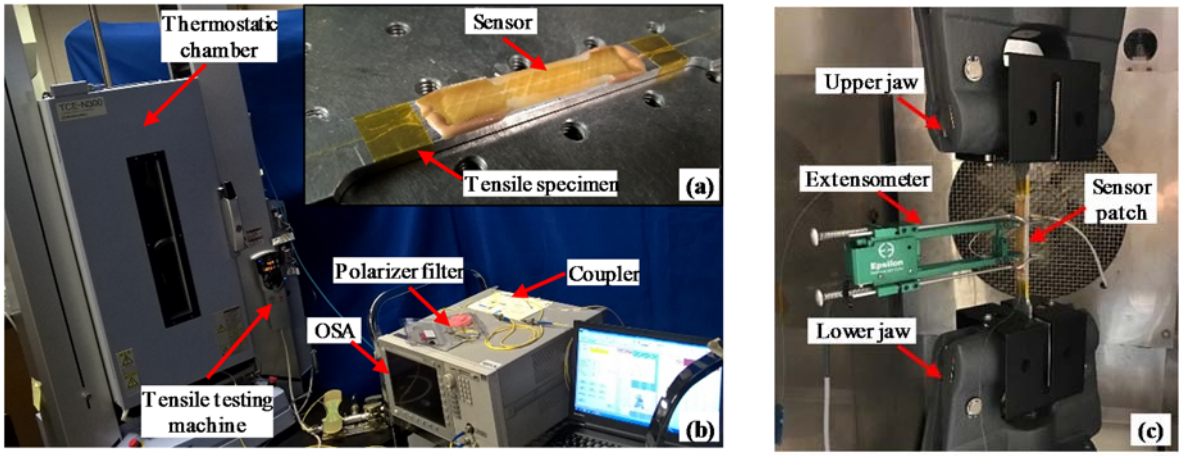

Figure 2.6. Thermal-mechanical testing of the sensor patch: (a) sensor patch bonded to the aluminum dog-bone; (b) experimental set-up; (c) sensor mounting inside thermostatic chamber.

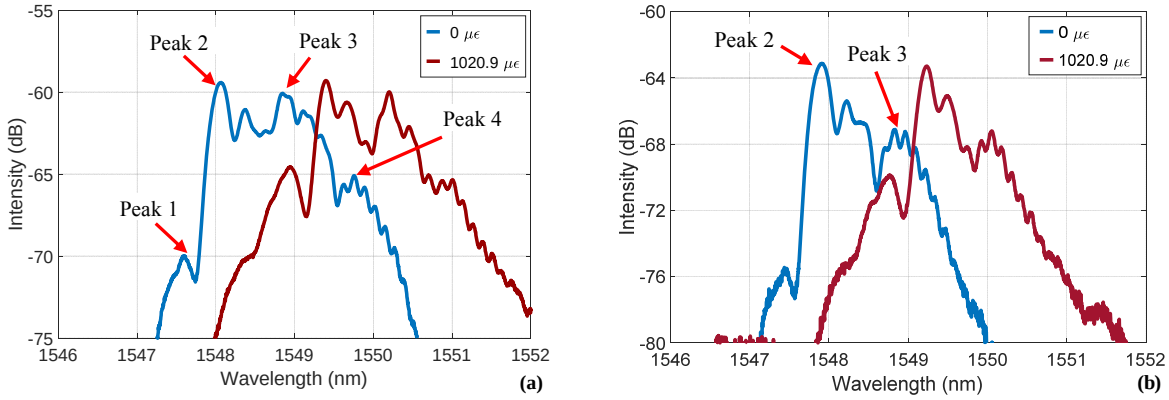

Figure 2.7. Comparison of FBG spectra at different strain levels and at a constant temperature of 35°C, acquired using; (a) unpolarized light; (b) polarized light.

increment of 500 N and with a loading speed of 10 N/s. A constant load was maintained at each increment for a period of 50 seconds, during which the spectrum readings with a frequency resolution of 2.44 pm were acquired by the OSA.

The reflectance spectra of the FBG-composite sensor at two different strain levels and a constant temperature of 35°C, acquired using unpolarized and polarized lights, are compared in figures 2.7(a) and 2.7(b). Similar to what is shown in figure 2.5, the FBG spectra acquired using the unpolarized light, *i.e.* without the polarizer and the polarization controller, contains multiple split peaks, as shown in figure 2.7(a). Under a strain level of 1029 με, the top portion of the spectra appears to have narrowed while the bottom portion of the spectra seems to have broadened. We also observed the growth in the intensity of peak 1 and the emergence of a new peak at a wavelength shorter than peak 1. These complicated spectra changes make it extremely challenging to determine the bandwidth and the Bragg wavelength of the spectra. Controlling the polarization of the interrogation light, on the other hand, enhanced the spectral response of the sensor significantly; the two peaks with lower intensities, *i.e.* peak 1 and peak 4, were substantially suppressed, resulting in an improvement on the finesse of the spectrum at full-width-quarter-maximum (FWQM). While the polarized light could not produce a spectrum with a single peak at the high strain level, it did increase the difference between the intensities of the dominant peak and those of the peaks with low intensities. These benefits of using polarized light for interrogating the FBG-composite sensor remain the same regardless of the strain and temperature loadings on the sensor.

The FBG spectra acquired using the polarized light can further be improved by removing the noise, *i.e.* the small ripples. For this purpose, a post-processing algorithm with a second order Butterworth digital filter was

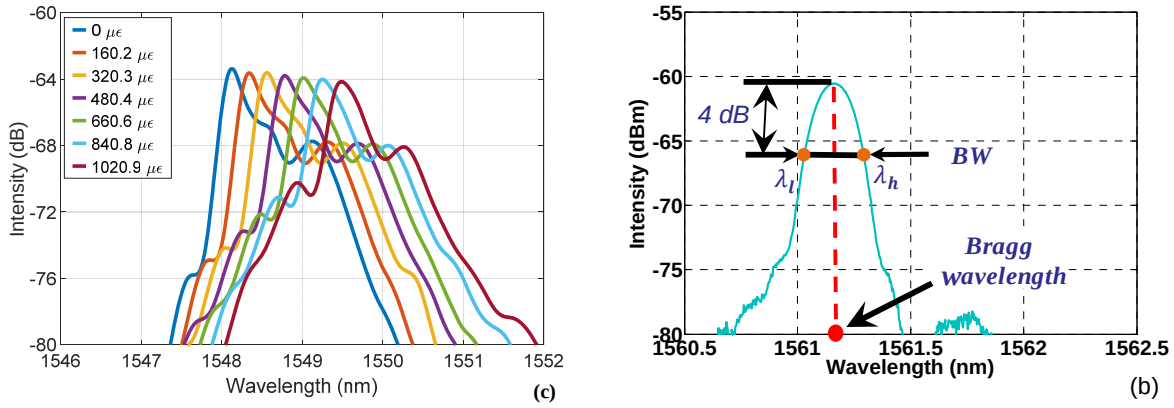

Figure 2.8. Post-processing of FBG spectra; (a) improved FBG spectra after applying digital filter to remove high frequency noise; (b) extracting the Bragg wavelength and bandwidth from the post-processed FBG spectrum.

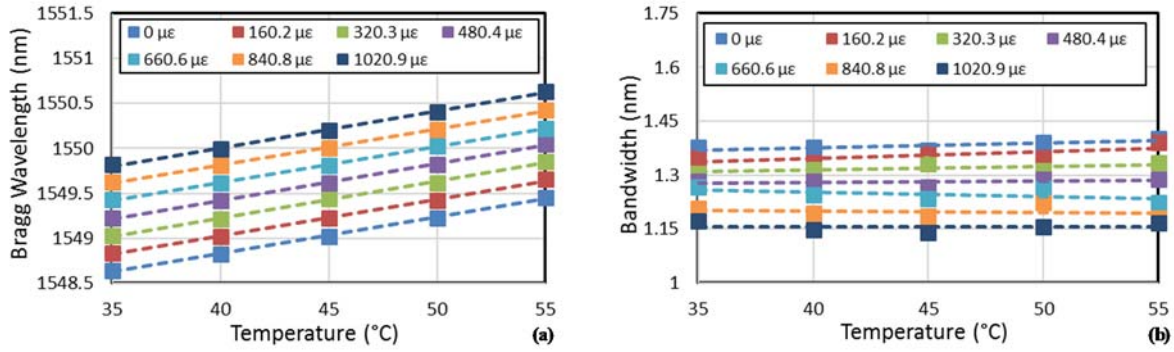

Figure 2.9. The shift in (a) central Bragg wavelength and (b) bandwidth with temperature variations at constant axial strains.

implemented. As shown in Figure 2.8(a), the filtered FBG spectra displayed a dominant peak; the central wavelength of this dominant peak shifted to larger wavelengths and its bandwidth decreased consistently with the increasing strain. To quantify these effects, a MATLAB program was developed to extract the Bragg wavelength and the spectral bandwidth from the post-processed FBG spectra. As shown in figure 2.8(b), two cut-off wavelengths, i.e. the low and high cut-off wavelengths, denoted as λ_l and λ_h, were identified at an intensity that is 4 dB below the peak intensity of the spectrum. The central Bragg wavelength was then calculated as $\lambda_B = (\lambda_l + \lambda_h)/2$, while the spectral bandwidth was calculated as the difference between these two cut-off wavelengths, *i.e.* $BW = \lambda_h - \lambda_l$.

The Bragg wavelength and the bandwidth, under constant strain, are plotted versus temperature in figure 2.9. As shown in figure 2.9(a), the Bragg wavelength increased linearly with increasing temperature for all strains. The wavelength-temperature curve under different strains are parallel to each other, indicating that the temperature sensitivity, measured as the slope of the wavelength-temperature curve, are similar for all strains. In other words, the applied strain seems to affect the intersection of wavelength-temperature curve but not its slope. The bandwidth, on the other hand, did not change much with temperature increase, especially when the strain level is high. The strain increase, however, did move the intersection of the bandwidth-temperature curve to a lower value, as shown in figure 2.9(b). The Bragg wavelength and the spectral bandwidth, extracted from the measured FBG spectra under different strain and temperature combinations, were plotted versus the applied strain and temperature in three-dimensional (3D) plots, as shown figure 2.10. Subsequently, the measured data were curve fitted using first order polynomials, which resulted in

$$BW(T,\varepsilon) = 0.00039T - 0.00022\varepsilon + 1.374, \quad (4)$$

$$\lambda_B(T,\varepsilon) = 0.0407T + 0.00114\varepsilon + 1547.211, \quad (5)$$

where T is temperature, ε is the applied strain in micron-strain, BW is the measured bandwidth, and λ_B is the measured Bragg wavelength. The temperature and axial strain can then be inversely determined from the measured bandwidth and Bragg wavelength as

$$\begin{bmatrix} T \\ \varepsilon \end{bmatrix} = \begin{bmatrix} 0.00039 & -0.00022 \\ 0.0407 & 0.00114 \end{bmatrix}^{-1} \left(\begin{bmatrix} BW \\ \lambda_B \end{bmatrix} - \begin{bmatrix} \\ 1547.211 \end{bmatrix} \right) \begin{pmatrix} ^\circ C \\ \mu\varepsilon \end{pmatrix}. \quad (6)$$

The differences between the strain and temperature values calculated using equation (6) and their actual values are presented in figure 2.11. As shown in figure 2.11(a), the measurement errors for the applied strain lie between -130 με to +100 με with a mean value of 0 and a standard deviation of 62 με. In other words, 68% of the strain measurement errors are within ±62 με. For temperature measurements, the measurement errors lie between -3°C

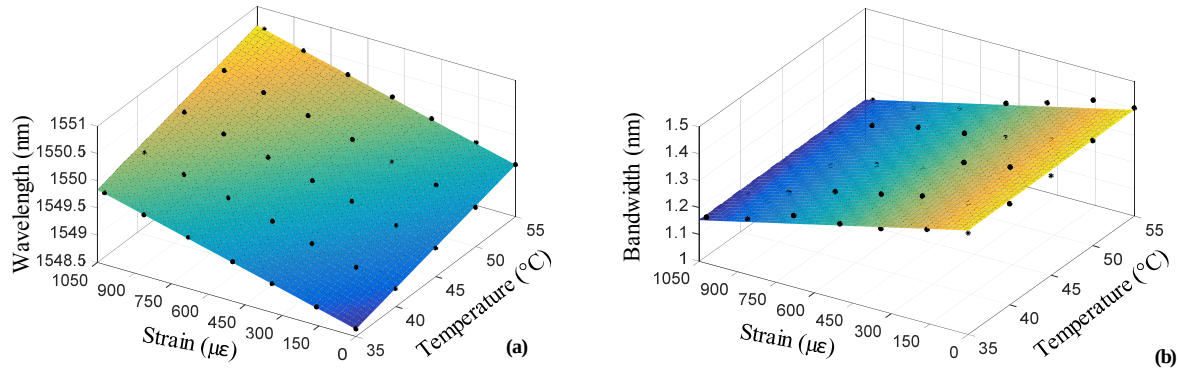

Figure 100. Curve fitting (a) the Bragg wavelength and (b) bandwidth as a bi-linear function of temperature and axial strain.

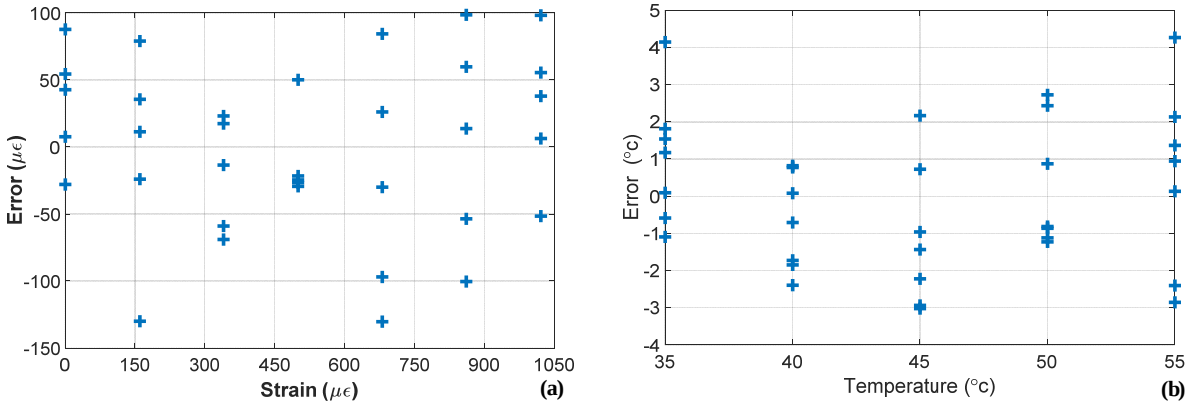

Figure 2.11. Differences between the measured and actual values; (a) axial strain; (b) temperature.

to 4°C and the standard deviation is ±1.94°C

Achievement Summary

1) Introduced the spectral bandwidth as an additional sensing parameter for strain-temperature differentiation;
2) Demonstrated simultaneous load and temperature measurements using a single FBG sensor coated with thermochromic material;
3) Demonstrated simultaneous strain and temperature measurements using a single FBG sensor embedded in a composite laminate;
4) Develop data analysis algorithm to inversely determine strain and temperature from the Bragg wavelength and the spectral bandwidth of an FBG sensor;
5) Develop techniques to improve the spectrum of the FBG sensor embedded in a composite laminate for data processing;

6) Published one journal paper and submitted a second journal manuscript;
7) Presented the research results at two conferences (i.e. 2016 ASME SMASIS conference and 2017 SPIE Smart Materials/Structures and NDE conference);
8) Graduate a Master's student.

Refereed Journal Articles

- Singh, A., Zhu, Y., Han, M. and Huang, H., 2016, "Simultaneous load and temperature measurement using Lophine – coated Fiber Bragg Gratings", v25, *Smart Materials and Structures*, 115019 (6pp)
- Singh, A., Zhu, Y., Han, M. and Huang, H., "Simultaneous strain and temperature measurement using a single fiber Bragg grating embedded in a composite laminate", submitted to *Smart Materials and Structures*

Books And Chapters

- None

Technical Reports

- None

Contributed Presentations

- A.K. Singh, Y. Zhu, M. Han, H. Huang, "Embedded fiber Bragg grating sensor for the simultaneous measurement of strain and temperature", SPIE-Smart Structures and Materials and NDE for Health Monitoring and Diagnostics, Portland, OR, March 2017
- A. Singh and H. Huang, "A single fiber Bragg grating sensor for the simultaneous measurement of strain and temperature", the ASME 2016 Conference on Smart Materials, Adaptive Structures and Intelligent Systems (SMASIS2016), Stowe, VT, Sept., 2016.

Patents

- None

Honors

- None

Related Sponsored Work

- None

ONR Statistics

Grad Students(total):	2
PI/Co-PI Women:	1
PI/Co-PI Minority:	0
Grad Students Women:	0
Grad Students Minority:	0
Post Docs Students:	0
Post Doc Women:	0

Post Doc Minority:	0
Under Grad Students(total:	0
Under Grad Students Women:	0
Under Grad Students Minority:	0
Degrees Granted:	1
Invention disclosures citing ONR support:	0
Other funding sources:	0